Study of the Free Surface Flow in the MICAS Mock-Up in Support of the ASTRID SFR Program.

David GUENADOU, Philippe AUBERT, Valérie BISCAY, Manon BOTTIN, Jean-Philippe DESCAMPS
Commissariat à l'Energie Atomique et aux Energies Alternatives
Cadarache, 13108 Saint Paul lez Durance
david.guenadou@cea.fr, phillipe.aubert@cea.fr, valerie.biscay@cea.fr, manon.bottin@cea.fr, jean-philippe.descamps@cea.fr

ABSTRACT

The CEA and several industrial partners are involved in the development of a 4th generation reactor cooled by sodium. This sodium fast neutron reactor called ASTRID (Advanced Sodium Technological Reactor for Industrial Demonstration) is a 600 MWe pool reactor type integrating cutting edge technologies. Developments are in progress especially for the vessel and the equipment. From the state of art of the previous mock-ups built in the 90s in the framework of the EFR program (European Fast Reactor), new needs for experimental means were listed for the ASTRID program. Experiments are needed for both validation of numerical codes and specific studies. In this way, a thermal-hydraulic loop, the PLATEAU facility, was developed and built at the CEA Cadarache research center. Different mock-ups, using water as a simulant fluid, can be connected to this loop to study the different issues at various reactor conditions. Currently, 4 mock-ups were identified: the hot plenum, the entire pool reactor, the link between the external and the hot plenum, a part of the hot plenum at a higher scale to study specific issues. The first model connected to the PLATEAU facility is MICAS, mock-up of the hot plenum. This one is dedicated to study the flow regime, both for code validation and also engineering design development. It was designed at 1/6 scale and was built in transparent polymer to carry out some optical measurements as laser velocimetry and fast imaging. The main issues identified for the upper plenum and studied on the MICAS mock-up are the thermal interface behavior around the core, the thermohydraulic stability and the flow distribution at the IHX inlet, the thermal and the flow pattern in the UCS and the free surface flow state. The first studies in the MICAS mock-up regard the free surface flow and the gas entrainment in the IHX. The experimental conditions (inlet flow rates, temperatures) are calculated to get the same Froude number as the ASTRID reactor. The vortexes at surface are studied using 3 cameras watching the same area in 3 different plans. A statistical analysis of the vortex is performed by imaging in term of life time, depth and width. The effect of the surface flow level is analyzed. The study is carried out at experimental conditions representative of nominal ASTRID power.

KEYWORDS

Sodium fast reactor, mock-up, vortex.

1. INTRODUCTION

The 4th generation nuclear reactors (GEN IV) are in development in all over the world. They aim at producing electricity with less nuclear wastes and safer. Moreover, a huge part of nuclear material not burnt in the GEN II and GEN III nuclear power plants, may be used as fuel in the GEN IV. The CEA is well experimented in sodium fast reactor with the RAPSODIE loop and the PHENIX reactor [1]. In the 90s, many studies were also carried out in the framework of the EFR project. Since 2010, the CEA and industrial partners have been involved in developing a new 4th Gen reactor: ASTRID (Advanced Sodium Technological Reactor for Industrial Demonstration). Its main objectives are to demonstrate

the technological feasibility and to prepare the industrial deployment of the GEN IV reactors [2]. The design options will be validated during the reactor operation, mainly in the field of the safety and the operability. ASTRID is a 600 MWe pool-type reactor cooled by sodium. This scale was chosen to be representative enough and to limit the cost. A scheme of the current design is shown on the Fig. 1. The sodium, heated in the core, is injected in the internal vessel (upper plenum). A part of the flow (around 15%) crosses the Upper Core Structure (UCS). This element maintains the control rods and the core instrumentation to monitot the outlet temperature and flow-rate of the fuel assemblies. The fluid crosses the 4 Intermediate Heat Exchanger (IHX) to heat a secondary sodium circuit and enters the external vessel (lower plenum). This solution was adopted to isolate the primary sodium from the water in case of leakage. Three primary pumps inject the sodium into the diagrid which distribute the fluid into the fuel assemblies.

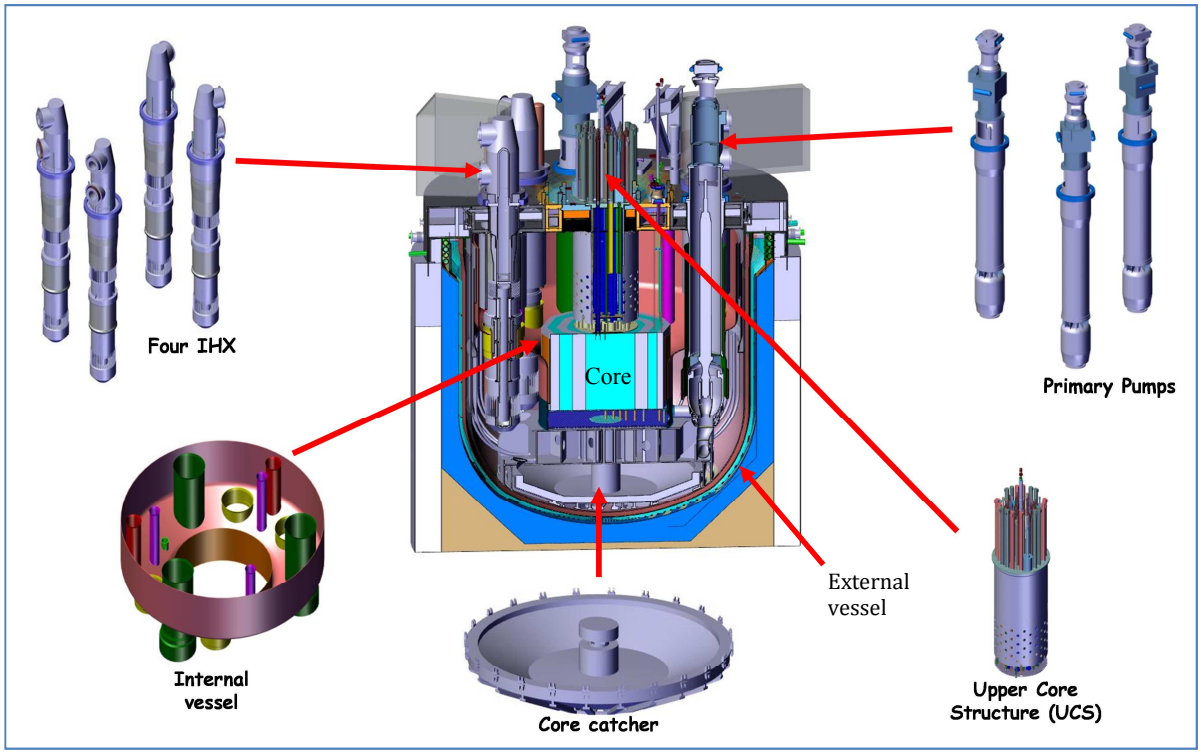


Fig. 1 Cut view of the ASTRID primary circuit.

One issue of the sodium pool-type reactor is gas accumulation in the diagrid. If a gas pocket created on the roof was ejected into the core, a positive reactivity effect would occur and may lead to safety problems. Gas accumulation origins were studied in details [3, 4]. A part is due to the vortices created at the free surface in the upper plenum. An argon blanket covers the sodium to avoid any contact with air and limit the temperature. Gas entrainment may occur at the tip of some vortices by various processes: bubbles may be pulled from the gas core tip; a gas column may be sucked into the IHX. Nevertheless, the vortex may occur at the surface without gas entrainment by creating a dimple. To design the upper plenum, it appears crucial to identify the hydraulic conditions creating vortices with gas entrainment. Many studies were carried to study the behavior of the vortex and the criteria of gas entrainment [5-8]. As sodium is not useful for experiment due to its opacity and its dangerousness, most tests were carried out with water or other harmless liquids. For analytical studies, the experimental setups are small vessels with transparent walls to visualize the vortex [6-9]. The vortices are created by pumping the liquid at the bottom of the vessel with various pipe diameters to impose the outlet velocity. Gas entrainment occurrence map was established depending on numerous parameters versus the vortex type (dimple, bubbles pulled at the gas core tip, full gas core). Nevertheless it appears that those maps are highly depending on the vessel geometry [8] and are not relevant for general case. Those experiments are well appropriate for CFD validation because of their simple geometry, but cannot be used to foresee the gas entrainment to establish design rules of the upper

plenum. This study has to be carried out in mock-ups at a sufficient scale, representative of the reactor geometry. For instance, Kimura et al. [5] analyzed the free surface flow in a 90° sector model at a 1/1.8 scale. Most vortices are Karman type and are created around the immerged components. A gas entrainment map was built taking into account the water level and the inlet velocity.
In the ASTRID reactor, two approaches are led in parallel to study the gas entrainment by vortex. The first one is based on one phase flow CFD calculations. The free surface is modeled by a symmetry boundary condition, and the vortex occurrence is determined by criteria calculated from the flow characteristic (velocity, circulation, water depth…) [10]. Those calculations need experimental validations. The second approach is based on large scale models with water as simulating fluid. The operating conditions are calculated using dimensionless numbers. For charactering the free surface flow behavior, the Froude number is employed.
This study focuses on studying the gas entrainment in the ASTRID upper plenum by charactering the vortices at the free surface around each IHX. The effect of the water level is investigated. The first part of this article is devoted to present the experimental model and the measurement setups. In the last part, the results are analyzed by considering the vortex sizes and the gas entrainment potentiality.

2. EXPERIMENTAL MODEL AND MEASUREMENTS SETUPS

The experiments are carried out in the MICAS mock-up [11]. This 1/6 scale model of the ASTRID upper plenum was built in transparent polymer for optical visualizations. On the photo of MICAS presented on the Fig. 2 and the scheme of Fig. 3, we can see the 4 IHX in the corners, the UCS in the center just above the core, the 3 pump pits (noted P0x), one decay heat exchanger (RR1a), and one inspection access during operation (ISIR3). The IHX geometry can be changed in term of opening elevation and height. The upper plenum model is surrounded by a 12 planes pool filled with water to limit optical deformations. The water level in the MICAS model is monitored by a guided wave radar sensor EMERSON Rosemont 5301 (accuracy +/- 2 mm). The mock-up is supplied by the PLATEAU loop at a 380 m^3/h maximal flow rate. The core is slit in 3 injection zones: the fission area, the reflectors and the internal fuel storage. In those zones, the flow rates are fitted according to the real flow distribution in the ASTRID reactor. The MICAS model and the PLATEAU facility are described in detail in [11].

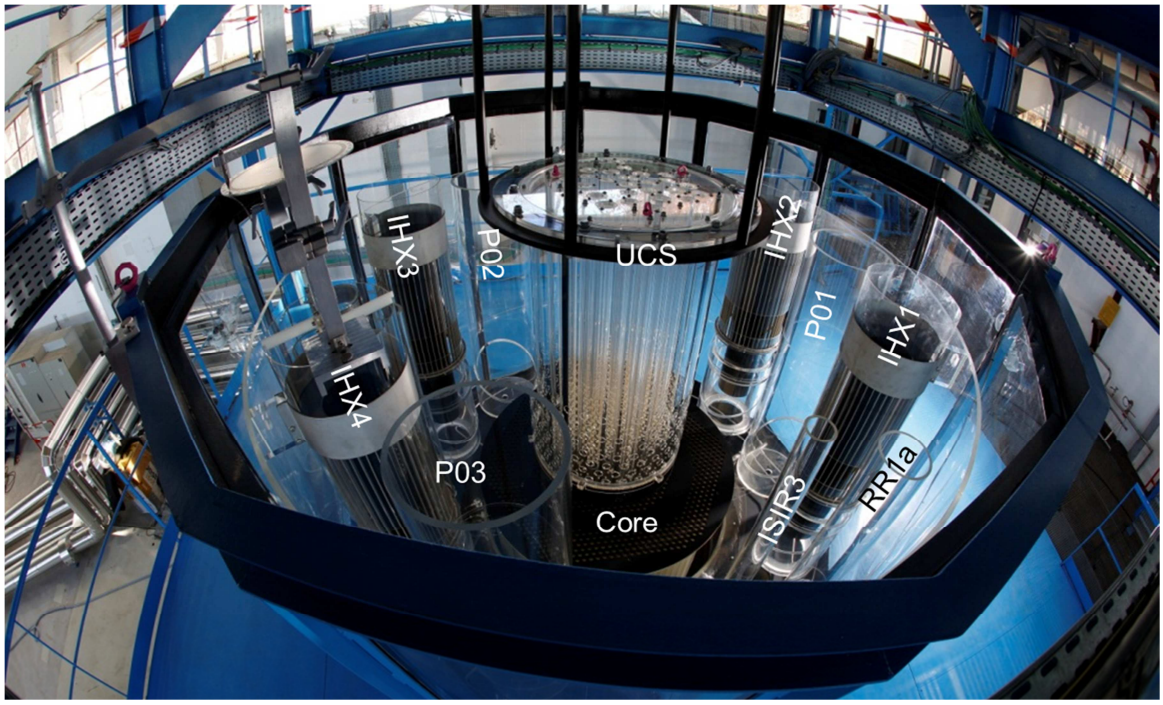


Fig.2 Top view of the MICAS mock-up.

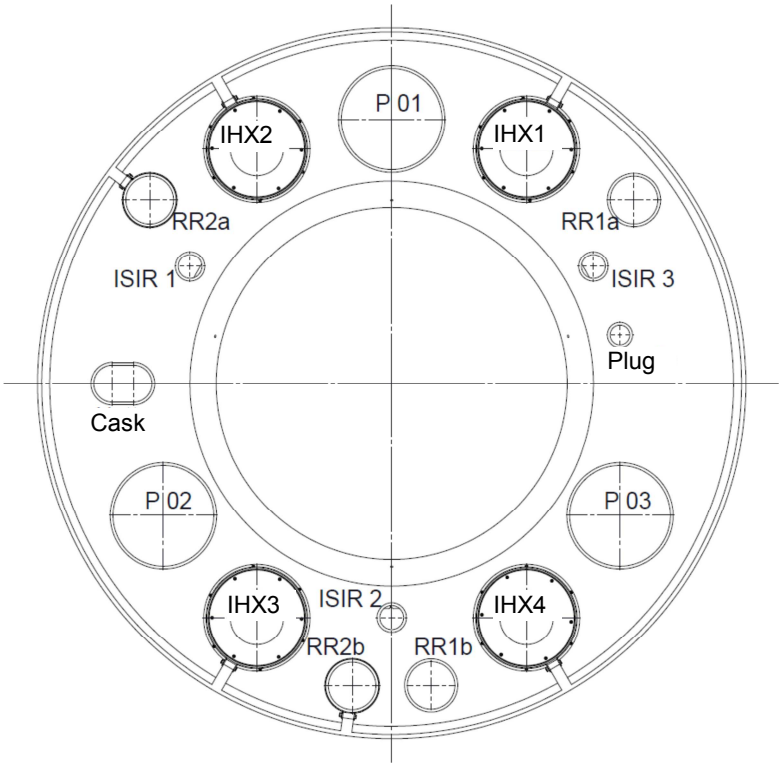


Fig.3 Location of the various immerged components in the MICAS mock-up. The core and the UCS are not shown.

The methodology to characterize the free surface flow was presented previously in [11]. As it requires the same Froude number in the reactor and the mock-up, the experimental operating conditions can be calculated. The gas entrainment is highly depending on the water head [9]: 3 levels are studied in the MICAS mock-up. The temperature also influences the gas core length as noticed in [9]. The water temperature was maintained at around 25°C using the chiller of the PLATEAU loop. Indeed, due to the heat losses in the circulating pump, the water temperature at model inlet tends to increase. The water inlet temperature is monitored by thermocouples (+/-1°C of accuracy) located in the PLATEAU loop. The operating conditions are summarized in the Table I.

Table I. Experimental operating conditions in the MICAS mock-up for studying the water level influence on the gas entrainment.

Temperature	20°C		
Flow rate	385 m^3/h	**Fission zone**	95.5%
		Reflectors	1.1%
		Internal Storage	3.4%
Water level	900 mm		
	786 mm		
	619 mm		

The water head 786 mm corresponds to the ASTRID nominal sodium level at the scale 1/6. In Table I, the null water level is defined at the top of the core.
The experimental procedure starts by establishing and stabilizing the operating conditions, especially the water temperature. As air is trapped in the PLATEAU loop and some gas is solubilized in water, a lot of little bubbles appear at the beginning of the operation. They have to be eliminated, as they can disrupt the analysis of the gas entrainment. The PLATEAU loop is fitted out with a liquid/gas separator. It allows eliminating most of the bubble after 1 hour of running.

The free surface flow is characterized by image analysis. As the vortices are created by a downward

flow, the interest study area is located around the IHXs. Two CMOS cameras (Proximage 250 SeeFast Technologies) are placed in front of each side of the IHXs (cf. Fig. 4). The acquisition rate is 60 frames per second to catch in details the vortices motion. This rate was evaluated to get as sufficient accuracy versus the video file size. Five minutes of recording time was chosen to get a statistical analysis of vortices size. It seems to be a good deal between the counted vortices, the analysis time and the file size. The cameras are fitted out with 50 mm lens (Hama) and the CMOS resolution is 640x480 pixels. The characterization of vortex was carried out using an images analysis software (EyeMotion upgraded with Graphics Tools 2D). To calibrate the images (pixel versus real length), a target is put in the vessel at the measurement location. Due to the camera field depth, all the objects located in a 50 mm depth box are net and can be taking into account for the study. From this statement, a measurement area can be defined around the IHX. The blue boxes in the scheme of the Fig. 5 present the investigation field. The different measurement volumes are noted on the Fig. 5 from V1 to V5 with the subscripts R or L to identify the right or the left side of the IHX. Their dimensions are reported on the Fig. 5. The area located next the UCS was not investigated because the length of the arm which handled the target was too short. Unfortunately, this area is known to be the birth place of numerous vortices. Further experiments will be led in this zone.

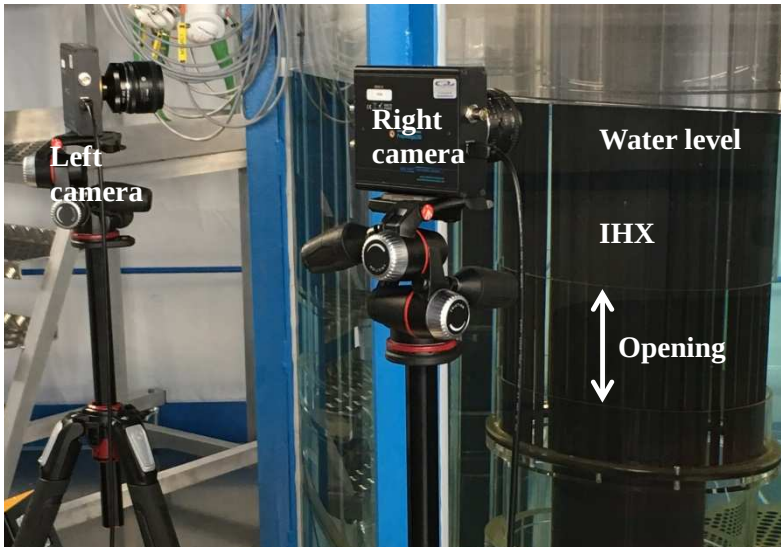


Fig. 4 Experimental setup to visualize the vortices at the free surface.

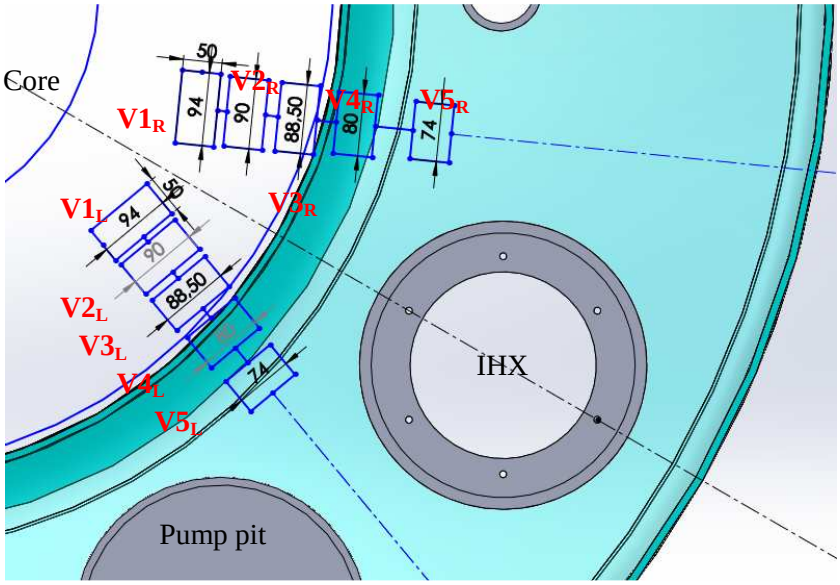


Fig. 5 Top view of the vortices investigation area in the MICAS model (dimensions in mm).

For each volume of the Fig. 5, the 5 minutes video are analyzed by only taking into account the vortex which sizes down to 2 mm depth. Every vortex is characterized in term of depth, diameter at mid-depth and life time in the camera field. As the vortex size is varying during its life, only the maximal values are reported. The accuracy is taking into account human error during the measurement on the software (+/-1 pixel, +/-0.1 s) and the error due to the measurement volume. Indeed, as we only analyze a 2D image, we do not know the exact vortex location between the foreground and the background of the measuring volume. But, as the target is placed at the center of the measuring volume, the vortex size is defined as if it was in the center plane. This error is calculated by subtraction of foreground and background calibrations in every measurement volume. Considering the calibration is depending on the location, the size accuracy varies according to the measurement volumes. The Table II reports the accuracy taking into account the human and the calibration error. Note that the accuracy is the same for the right and the left side of the IHX. In the Table II, we can notice that accuracy is better near the IHX and worst near the core.

Table II. Size accuracy in the measurement volumes

Measurement volume	V1	V2	V3	V4	V5
Accuracy (mm)	1.5	1.4	1.3	1.2	1.1

3. EXPERIMENTAL RESULTS AND DISCUSSION

3.1 General behavior of the free surface flow

From the general point of view, the vortices are rather small. Most of them are less deep than 10 mm. But as observed during the EFR project [4] small scale models tends to under-estimate the vortex size. This study will provide some trends about the locations with a high vortex probability occurrence. The average size of the vortex is 25 mm in diameter and 4 mm in depth. Two kinds of vortex are displayed on the Fig. 6. The left photo exhibits a developed vortex where we can notice the coherent swirl. The movie recorded during the test shows some bubbles pulled from the core tip. We did not notice if the gas was entrained into the IHX, but nevertheless the gas volume entrained was very low, the vortex living a very short time. During the whole experimental program, only few of this kind of vortex are noticed. Most of the vortices are dimple shaped as presented on the right photo of the Fig. 6. No gas entrainment can occur with this kind of vortex. The common vortex classification [4] exhibits 6 kinds of vortex, but during this experimental campaign, we observed all types except one. We noticed small dimples (type 2) to vortices pulling air (type5), but no full air core (type 6).

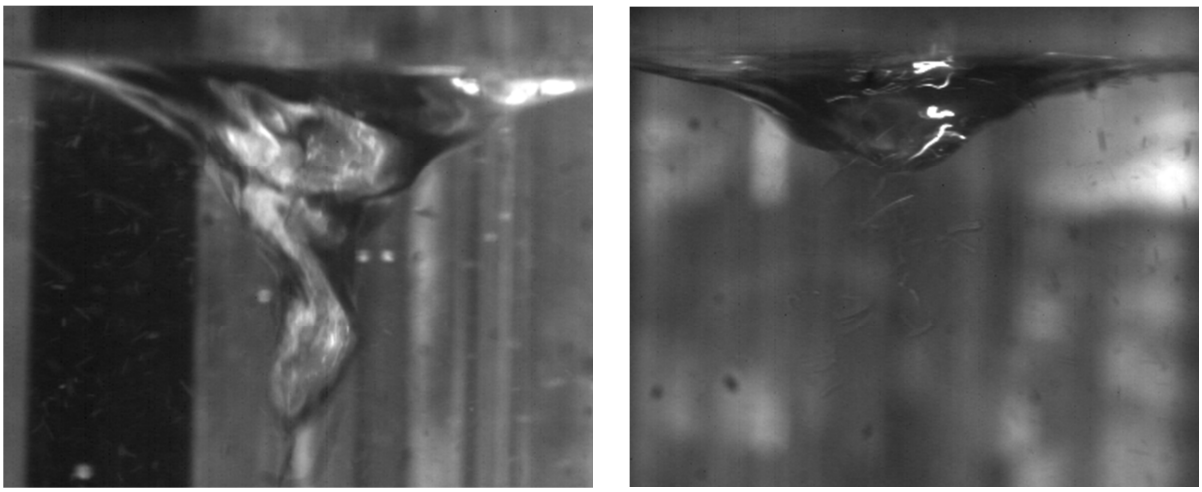


Fig. 6 Photo of different vortex types observed

3.2 Influence of the water level

During its operation, the reactor sodium level may mainly vary because of power change (up or down). It may also decrease due to a leakage. For those reasons, it seems important to study its influence on the free surface behavior. For each studied level, a count of the total vortex around all the IHX was carried out. The overall average size in terms of diameter, depth and diameter at mid-depth was calculated for each level. The graph of the Fig. 7 presents the results. As we can see on this graph, the vortex size changes a little depending on the water level. The vortex depth tends to decrease as the level increases. It seems coherent, because at low level, the free surface is closer to the intake (the IHX opening) where the downward velocity is high. Regarding the diameter, a maximum is reached at a value of 786 mm, i.e. the nominal level. We had expected the diameter would be correlated to the depth. It may be due to the lack of accuracy of our measurement. As we can see on the Fig. 7, the error bars at the levels 619 and 786 mm are in the same range.

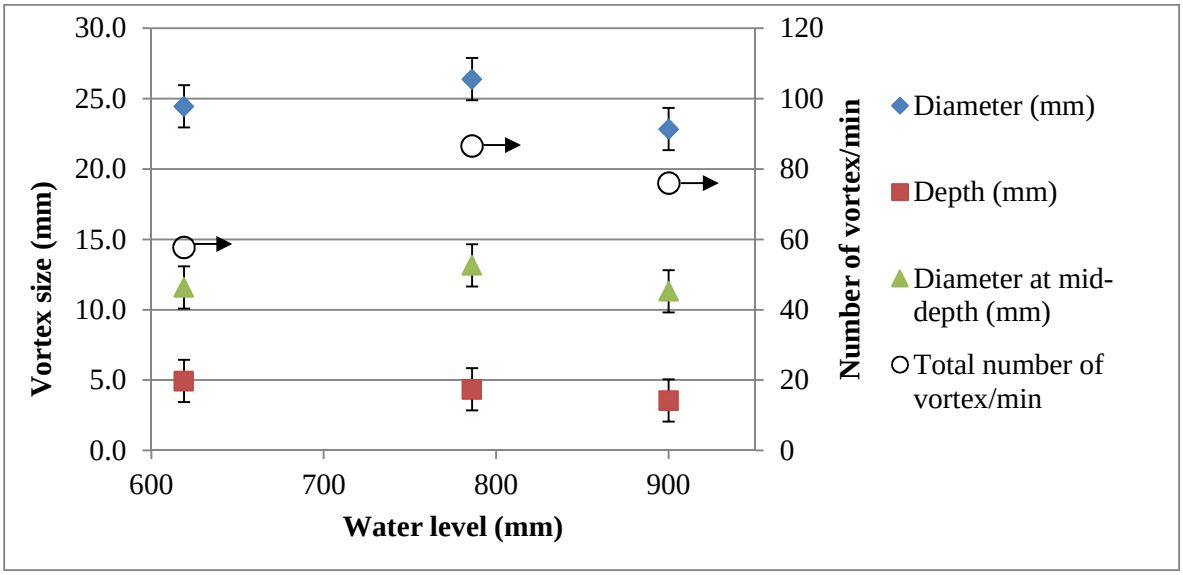


Fig. 7 Size and amount of vortices around the 4 IHX depending on the water level.

The empty black circles of the Fig. 7 shows the amount of vortices deeper than 2 mm which occur around the 4 IHX. For this value, it's rather difficult to estimate the accuracy as the count is carried out by a human operator. Some vortices may be omitted due to the under-estimation of the depth (only the vortex deeper than 2 mm are counted), the uncertainties of its occurrence inside the measurement volume (the vortex are displayed net inside and more or less blur outside), the lifetime which can be too short to be noticed. But to evaluate the accuracy and the reproducibility, some tests were carried out twice. The results are summed up in the Table III. As we can notice in this table the results are quite closed between the two tests. So we can conclude that the reproducibility and the accuracy of the vortices count are quite good. On the Fig. 7, we can notice the maximum amount of vortices occurs at the nominal level, i.e. 786 mm. This factor is correlated with the maximum diameter. Like previously for the diameter, we had expected that the maximum count would happen at the lower level. Surprisingly, the minimum vortex amount occurs at the lower level. The vortex amount gives an idea of the free surface flow behavior, but it is not the accurate indicator to study the gas entrainment potentiality. Indeed, the gas entrainment is linked to its lifetime and its size. If a lot of vortices occurred with a short lifetime, the air entrainment probability would be very low. So to determine the effect of the lifetime the occurrence factor f is defined in the equation (1). It gives the occurrence probability of vortices.

$$f = 1/T \sum t \quad (1)$$

Where T is the overall visualization time and t is lifetime of the vortices.
According to the equation (2), this occurrence factor can also be defined depending on the vortex category in terms of range of diameter and depth.

$$f_{d1<d<d2}^{\emptyset 1<\emptyset<\emptyset 2} = 1/T \sum t_{d1<d<d2}^{\emptyset 1<\emptyset<\emptyset 2} \quad (2)$$

Where $t_{d1<d<d2}^{\emptyset 1<\emptyset<\emptyset 2}$ is lifetime of the vortices whose diameter is between ø1 and ø2 and whose depth is between d1 and d2.

Table III. Vortices count reproducibility tests

Water level (mm)	IHX	Amount of vortices/min	
		Test 1	Test 2
619	1	13.6	13.6
619	3	14.6	14

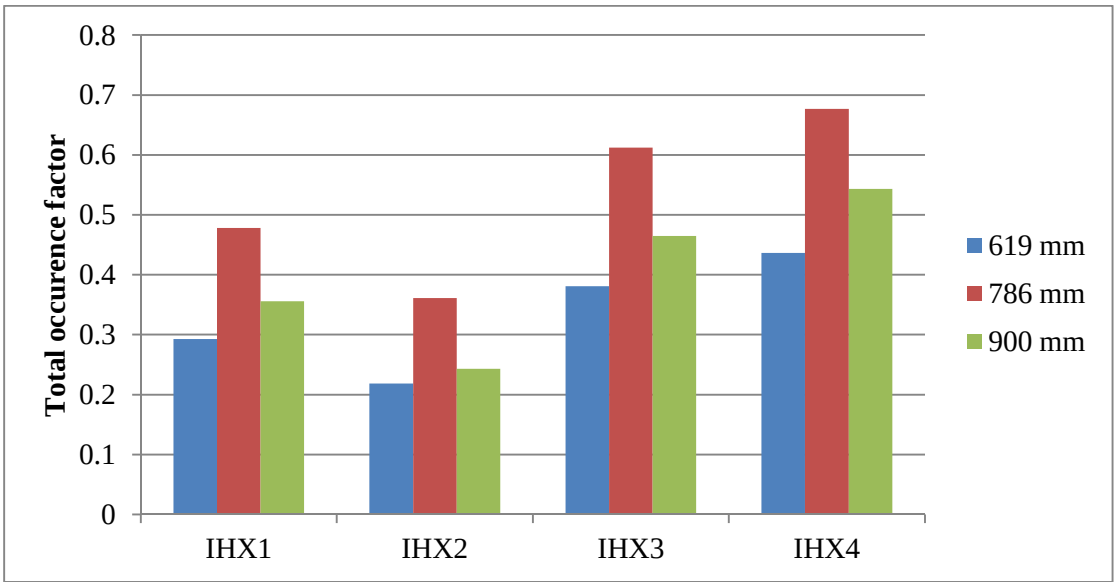


Fig. 8 Vortex occurrence factor depending on the IHX and the water level

The Fig. 8 shows the overall occurrence factor calculated according to the equation (1) and depending on the IHX and the water level. First of all, we can notice that the trends established in the previous paragraph on the level influence are well confirmed. The nominal level exhibits the highest occurrence factor whatever the IHX and the minimal value is noticed at the lowest level. On the Fig. 8, we can rank the occurrence factor according to the IHX: IHX4, IHX3, IHX1, IHX2. The classification is not depending on the level. While IHX3 and IHX4 are quite in the same range, IHX2 is rather below IHX1, but we can identify two main behaviors. The two areas around the IHX3 and IHX4 exhibit a high potentiality of vortex occurrence, while the areas around the IHX1 and especially IHX2 shows a light probability. According to [5], the main source of vortices is due to Von Karman vortex created around the immerged components. Indeed, the flow out-coming from the core is deflected up on the vessel wall to the free surface. At the surface, the water moves radially to the center vessel and go down when it meets the UCS. When the fluid flows around an immerged obstacle, some Von Karman vortices are created downstream and transported by the flow. We can notice on the Fig. 3 that the IHX3 and IHX4 are surrounded by numerous immerged components. Even if symmetry can be found between the IHX (all of them are surrounded by a pump pit and two decay heat exchangers), the space between the IHX3 and the IHX4 is more congested. The three tubes ISIR2, RR2b and RR1b have an influence on both IXH3 and IHX4. All those components are a source of vortices. This kind of structure does not exist on the other side for IHX1 and IHX2.

On the Fig. 8, we may notice that even if IHX1 and IHX2 exhibit close occurrence factor values, IHX2 is a little below. The same fact can be noted for IHX3 and IHX4. We may express a hypothesis to explain this little difference of behavior between IHX3 and IHX4, and between IHX1 and IHX2. On the Fig. 9, we can see the decay heat exchangers RR2a and RR2b are hung by a lug stuck on the vessel and do not touch at their bottom the conical part of the upper plenum. As illustrated on the Fig. 9, the

water can flow between the bottom of those components and the vessel wall. On the contrary, the RR1a and RR2a are stuck on the conical part of the vessel. As the water flows around those tubes as shown on Fig. 9, some Von Karman vortices may start to be created. On Fig. 3, the decay heat exchangers RR1a and RR2a are located close to the IHX1 and IHX4. It may explain why they exhibit little more vortices than respectively IHX2 and IHX3.

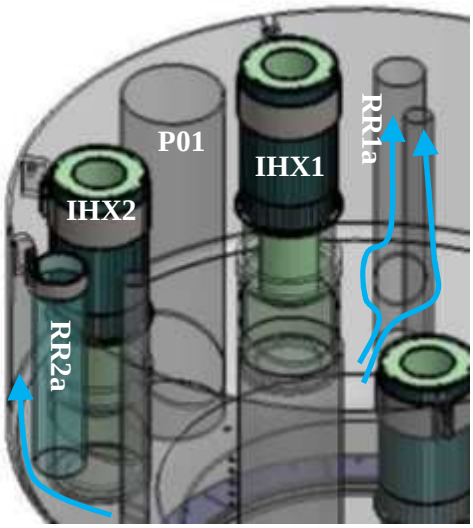


Fig. 9 Streamlines around the decay heat exchanger RR2a and RR1a

As 786 mm is the nominal level and it exhibits the maximum of vortices, we focus our investigations on this level.

3.3 Vortex analysis at the nominal water level

The previous paragraph has shown that the IHX4 and IHX3 exhibit the maximum occurrence factor. Nevertheless, the air entrainment is not only depending on this factor; it is also correlated with the vortex size. Actually, we cannot forecast at which vortex size air entrainment occurs, but the bigger is the vortex, the higher is the risk. A model has been developed to foresee the gas entrainment probability but it requires the vorticity profile at the free surface [10]. To assess the gas entrainment probability, we calculated around all IHX the occurrence factor depending on the vortex size according to the equation (2). The results are presented in the Fig. 10 as 2D colored maps with the same scale for the 4 IHX. First of all, we can notice that the most probable vortex category is same for all IHX: a diameter ranged from 5 to 15 mm and a depth sized from 2 to 5 mm. It's coherent with the mean sizes reported on the graph of the Fig. 7. On the Fig. 10, we can observe two main trends: the maps patterns are similar between IHX1 and IHX4, and between IHX2 and IHX3. IHX1 and IHX4 exhibit deeper vortices than IHX2 and IHX3. It may be explained by the same reasons we argued in the previous paragraph. IHX2 and IHX 3 are close to tubes (RR2a and RR2b) which are not in contact with the vessel wall. The decay heat exchanger RR1a and RR2b seem to be the origin for the development of deeper vortices. Velocities measurements have to be carried out to confirm this hypothesis. Even if the overall occurrence factor of IHX1 is smaller than the value of IHX3 (see Fig. 8), the gas entrainment probability may be higher due to the occurrence of deeper vortices. Finally, when we compare all the results of the Fig. 10, the highest potentiality of gas entrainment is still around the IHX4 because of the widest occurrence factor map.

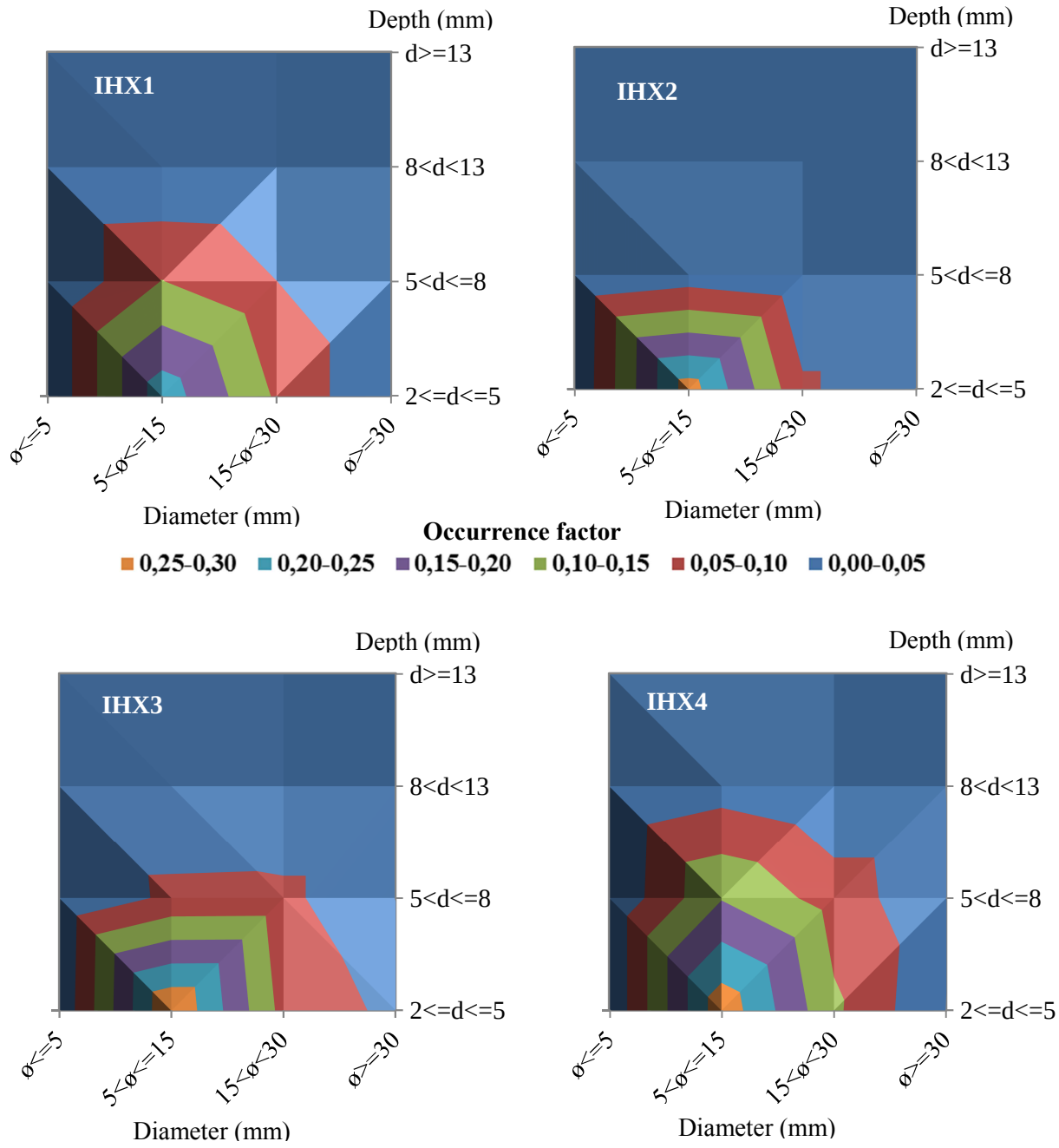


Fig. 10 Occurrence factor depending on the vortex depth (d in mm) and diameter at mid-depth (ø in mm) at the water nominal level.

3. CONCLUSIONS

The 1/6th scaled MICAS mock-up is dedicated to study the free surface flow in the upper plenum of the ASTRID reactor. This study was carried out at the same Froude number among the reactor and the model to get a similar surface flow behavior. Air entrainment is characterized by analyzing the vortices occurrence at the surface around the IHX using two rapid cameras. A statistical analysis of the vortex is performed by imaging in term of amount, life time, depth and width.

From the general point of view, the vortices observed during this experimental program are rather small even if some full developed swirl type vortices are noticed. Moreover, no gas core type is reported.

The water level influences a little the mean diameter and the depth of the vortices. At the lowest level,

we may notice a slight increase of the depth due to higher downward velocities. The highest amount of vortices occurs at the nominal level. A detailed analysis is carried out using the occurrence factor which accounts for the birth probability of the vortices. It is defined in an overall manner, by taking into account all the vortices, and in a statistical approach by size ranking. The results are observed, the level influences the occurrence factor in the same way.
The IHX3 and IHX4 show a high probability of vortex occurrence. The vortices are mainly created by Von Karman swirl around immerged structures. As IHX3 and IHX4 are surrounded by numerous tubes, it may explain the observed high values.
At the nominal level, the vortex occurrence depending on the size exhibits that the most probable vortex category is same for all IHX. Two main trends are noticed among the IHX. IHX1 and IHX4 show deeper vortex occurrence compared to IHX2 and IHX3. It may be explained by the geometry of the decay heat exchangers close to the IHX. As the RR1a and RR1b are in contact with the bottom vessel wall, they are place of birth of Von Karman swirls which may enhance the vortices at the surface. Velocities measurement will be carried out with a PIV system. This analysis must be compare to results. Finally, the highest potentiality of gas entrainment is still around the IHX4.

REFERENCES

1. J. Kremser, A. Lacroix, “Some Aspects of Sodium Technology Issued from the Operating Experience of RAPSODIE and PHENIX”, *Proceedings of the international conference on liquid metal technology in energy production*, Champion, Pennsylvania, May 3–6, 1976.
2. P. Le Coz, J.-F. Sauvage and J.-P. Serpantie, “Sodium-Cooled Fast Reactors: the ASTRID Plant Project”, *Proceeding of ICAPP 2011*, Nice, France, May 2–6, 2011.
3. D. Tenchine, “Some Thermal Hydraulic Challenges in Sodium Cooled Fast Reactors”, *Nuclear Engineering and Design*, **240**, pp. 1195-1217 (2010).
4. D. Tenchine, C. Fournier, Y. Dolias, “Gas entrainment issues in sodium cooled fast reactors”, *Nuclear Engineering and Design*, **270**, pp. 302-311 (2014).
5. N. Kimura, T. Ezure, A. Tobita, H. Kamide, “Experimental Study on Gas Entrainment at Free Surface in Reactor Vessel of a Compact Sodium-Cooled Fast Reactor”, *Journal of Nuclear Science and Technology*, **45**(10), pp. 1053-1062 (2008).
6. G Caruso, L Cristofano, M Nobili, D Vitale Di Maio, “Experimental Investigation of Free Surface Vortices and Definition of Gas Entrainment Occurrence Maps”, 31st UIT (Italian Union of Thermo-fluid-dynamics) Heat Transfer Conference, Como, Italy, June 25–27, 2013.
7. T. Ezure , N. Kimura , K. Hayashi, H. Kamide, “Transient Behavior of Gas Entrainment Caused by Surface Vortex”, *Heat Transfer Engineering*, **29**(8), pp. 659-666 (2008).
8. B. Moudjed, J. Excoffon, R. Riva and L. Rossi, “Experimental Study of Gas Entrainment from Surface Swirl”, *Proceedings of NURETH16*, Chicago, Illinois, August 30–Sept. 4, 2015, pp. 1033-1040 (2015).
9. H. Monji, T. Shinozaki, H. Kamide, T. Sakai, “Effect of Experimental Conditions on Gas Core Length and Downward Velocity of Free Surface Vortex in Cylindrical Vessel”, *Journal of Engineering for Gas Turbines and Power*, **132**, (2010).
10. T. Sakai, Y. Eguchi, H. Monji, K. Ito, H. Ohshima, “Proposal of Design Criteria for Gas Entrainment from Vortex Dimples Based on a Computational Fluid Dynamics Method”, *Heat Transfer Engineering*, **29**(8), pp. 731-739 (2008).
11. D. Guenadou, I. Tkatshenko and P. Aubert, “Plateau Facility in Support to Astrid and the SFR Program: an Overview of the First Mock-Up of the Astrid Upper Plenum, Micas”, *Proceedings of NURETH16*, Chicago, Illinois, August 30–Sept. 4, 2015, pp. 5861-5872 (2015).